A SUITE OF MODELS FOR PRODUCING SYNTHETIC, SMALL-SCALE THERMAL IMAGERY OF VEGETATED SOIL SURFACES

S. E. HOWINGTON[1], J. F. PETERS[1], J. R. BALLARD[1],
L. N. LYNCH[1], J. P. HALLBERG[1], AND C. E. KEES[1]

[1]Engineer Research and Development Center, Vicksburg, MS, U.S.A. 39180

Abstract

A high-resolution, computational suite has been constructed to produce synthetic thermal imagery of vegetated soil surfaces. Because soil moisture affects thermal response, the model suite must include both moisture and energy movement within the soil and plants. Thus, the suite consists of a soil model, a vegetation model, and a ray-casting model. The models run simultaneously on a single, parallel or serial computer and communicate using sockets.

The soil model is a three-dimensional, spatially adaptive, continuous Galerkin, finite element model that simulates partially-saturated flow and heat transport, coupled to two-dimensional surface water flow. The vegetation model simulates infrared absorption, reflection, and transmission by discretized plant leaves and stems. Ray casting provides boundary conditions for the soil and vegetation thermal models, and produces multi-spectral images of energy reflected and emitted from the synthetic scene. Subsurface phase change, distributed root zone moisture uptake and transpiration, and flow through macropores and cracks are processes under construction.

Example calculations to be presented include a multi-million-element simulation for an arid test site that is only a few meters in its longest dimension. The models are driven with meteorological data and are built using material property data collected at the field site. Synthetic images produced are compared against those from thermal cameras. A long-term goal of this work is to help build inversion software to estimate ground state information (soil moisture and physical property distributions) from airborne imagery.

1. Background

A computational tool is under construction to help understand the interaction of infrared (IR) sensors and the natural environment. One goal is to explore thermal and hydrologic process interaction at the scale of individual plants. A tool of this sort will permit analysis of microhabitat, study of desertification processes, and testing of homogenization techniques to explore fine-scale process expression at coarser scales common to remote sensing. Moreover, with a credible, physics-based 'forward' modeling tool to produce sensor imagery comes an opportunity to exploit sensor images to estimate ground state (soil moisture, soil or vegetation temperature or contrast) and material properties (hydraulic and thermal), even using sensors not designed or optimized for that purpose. This paper gives a brief overview of the testbed and a few results.

2. Testbed Components

The computational testbed is a collection of interdependent models and utilities. Energy inbound to the scene is tracked from direct solar and downwelling longwave sources. Energy is reflected, absorbed, and emitted by vegetation, soils, and other objects in the scene. The reflected and emitted energy is tracked back through the atmosphere and the sensor to produce an infrared image. Interactions among the models range from a 'tight' coupling, normally internal to a single code, to episodic boundary condition swapping, to one-directional file handoff.

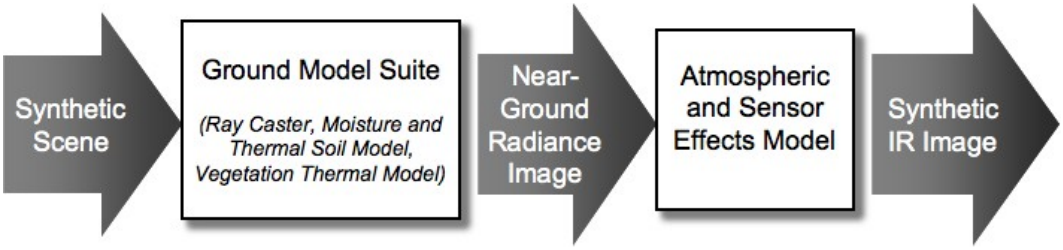

Figure 1. Overall data flow through the testbed. The focus here is on the ground model suite and production of the near-ground radiance image.

2.1. **Ray caster model.** The testbed is organized around the ray caster model, which directs the flow of energy among the entities of the model components. Direct solar energy and indirect solar energy is cast to all exposed surfaces and define the incident energy for the vegetation and ground models. Radiant energy emitted from surfaces is cast to neighboring surfaces. Reflected and emitted energy is cast to the sensor.

The ray caster carries information about the surface geometry of all entities in the test bed. The vegetation and ground models provide to the ray caster data in the form of three-vertex facets that define all surfaces and the materials that make up those surfaces. The ray caster assembles the facet data from each model component into a master description. Objects, such as leaves, which are translucent, are modeled by twin facets. The vegetation model depicts leaves by single facets which are visible from both sides. Facets in the ray caster are visible from only one side. Therefore, for translucent materials the ray caster pre-processing program duplicates these facets, but with their opposing side made visible, and identifies facet twins in a separate data array. Thus, when routing energy, a portion of the energy not reflected can be transferred to the twin facet as transmitted energy. Data on direct and indirect solar loading, sun orientation, and down welling thermal loading is obtained from the meteorological data base and assembled in a 'light' file. Also included in this file is the frequency content of the visible and thermal energy. The source files from these data as well as sensor-specific data such as view orientation and frequency bands of interest are provided to the ray caster in a scripting file.

The ray caster differs from those used for visualization in that the boundary flux must be determined for all surfaces and not just those visible to the sensor. Therefore, the energy is routed from the light sources to all exposed surfaces rather than from the sensor to surfaces to light source as it would be if only visualization was of interest. The basis of the ray caster is a simple visible surface algorithm using z-buffers. Several z-buffers

are maintained to route the various components of energy. For each light source, energy is compiled into a pixel array upon which the exposed surfaces are projected. Exposure of a surface is determined by the closest surface projected on the pixel. The incident energy is compiled into the facet total which can then be transmitted to the other model components as part of the energy flux boundary condition. Therefore, resolution of the energy input is determined by the facet size.

The ray caster provides the energy flux to the other test bed components as a facet-based list. In turn, each component returns to the ray caster physical temperatures at the vertices of the facets. Reflected energy from the lighting pixel array is projected on a similar pixel array defined by the viewing (sensor) orientation. Energy is compiled into a pixel from a surface that is exposed to both viewing array and lighting array. In this way, shadows are resolved to the resolution of the pixel size. Added to this energy is thermal energy emitted from the surface as computed from the temperature. The temperature is interpolated to the pixel location from the values at the facet's vertices. Energy transmitted through materials is compiled from twin facets in a similar manner. The viewing pixel array thus receives energy from both thermal and visible sources.

All operations with energy is wavelength dependent. To accommodate this dependency, energy is stored as six integers ranging in value from 0 to 1024 W/m^2. Each integer represents the energy within a band. Properties for reflectance, transmittance, and emissivity are likewise expressed by six components. Energy transfer operations are performed band-wise. Therefore, the ray caster logic contains no wave-length dependence. The physical meaning of each band is controlled by the values of contained in the material property and light files. Greater or lesser frequency resolution can be obtained within particular bands depending on these data. Moreover, computations of boundary flux need not use the same energy information as the final ray casting to the sensor. Thus, for example, the computation of boundary flux might use energy averaged over a wide range of frequencies, while the final ray casting to the sensor can place resolution in the narrow bands of interest for the sensor being simulated.

2.2. **Moisture/thermal model.** A key component of the energy balance is heat emitted or absorbed by the soil. For imagery, only the behavior at the ground surface is of interest. But, heat transport must be modeled in three dimensions to capture the surface expression of subsurface heat transport processes. Thermal properties depend on a soil's moisture content. Exploring the effect of hydrologic processes requires that water movement be simulated as well. Moisture and thermal energy movement in the soil is computed with the ADH (Adaptive Hydraulics/Hydrology Model) (*Schmidt,* 1995). The model includes local refinement and coarsening (h refinement only) of the computational mesh based on error indicators.

Moisture movement through the soil is estimated by solving Richards' equation in three dimensions (Equation 1) using a traditional, continuous Galerkin, finite element method on tetrahedra. The model also includes surface water equations to approximate runoff, puddle development, ponding and infiltration. Choices of surface water flow equations include kinematic wave, diffusive wave, and full shallow water. The groundwater and surface water are coupled and exchange fluxes each time step.

$$S_S S(\psi)\frac{\partial \psi}{\partial t} + \eta\frac{\partial S\left(\psi\right)}{\partial t} = \nabla \cdot \left[K_S k_r\left(\psi\right)\nabla\left(\psi + z\right)\right] + W \tag{1}$$

where ψ is pressure head, S_S is the specific storage, which accounts for water compressibility and aquifer elasticity, $S\left(\psi\right)$ is the water saturation or volumetric fraction of pore space occupied by water, η is the porosity or volumetric void fraction, K_S is the water-saturated hydraulic conductivity, k_r is the relative permeability of the media, and W is a source/sink term. In this formulation, the z axis is the vertical direction oriented positively upward. Both S and k_r are functions of ψ. K_S and S_S are provided as data.

An energy balance equation to simulate heat conduction, convection, and surface heat exchange was added to the moisture model. Thermal energy is transported by a standard conduction and convection equation

$$(\rho c)_m\frac{\partial T}{\partial t} + (\rho c)_f v \cdot \nabla T = \nabla \cdot (K_T \nabla T) + q_m \tag{2}$$

where ρ is density, c is specific heat, T is temperature, v is flow velocity, K_T is thermal conductivity, and q_m is a source of energy. Mixture coefficients are computed by volumetric averaging of components for thermal conductivity and mass averaging of components for specific heat. Specific heat and thermal conductivity depend on the soil moisture. Surface heat exchange includes short-wave input, longwave input, longwave emitted, sensible heat, latent heat, and precipitation heat (*Frankenstein and Koenig,* 2004).

2.3. **Vegetation model.** To understand the role of the energy budget components in a canopy-soil system we modeled the vegetation as discrete elements over the soil mesh. The vertical variations of the energy budget for the discrete vegetation elements are described in terms of the net radiation (R_n), sensible (convective) (H), and latent heat (LE), and ground heat flux (G). The energy budget is given as

$$R_n - LE - H - G = 0 \tag{3}$$

The temporal variations of sensible and latent heat fluxes are modeled as a function of vertical position of the discrete vegetation element by linking the latent and sensible heat fluxes to the measured wind speed and relative humidity. The near surface wind and relative humidity profile is based on a model driven by the measured wind and humidity. Solving the energy budget for each element at each time increment provides information on the vertical and temporal variation of vegetation element temperature, latent heat flux, and sensible heat flux. The latent heat modeled as

$$LE = \lambda(T_v)\frac{\rho_v^* - h_a\rho_a^*}{r_s + r_a} \tag{4}$$

is coupled to the wind speed and relative humidity just above the vegetation through to the vegetation discrete element and is dependent on vapor density ρ_v and aerodynamic resistance r_a. The latent heat also depends on the air density at a specified humidity $h_a\rho_a^*$, the saturation vapor density in the canopy ρ_v^*, and the element layer modeled stomatal resistance r_s. The stomatal resistance sub-model is modeled using the air temperature, relative humidity, global radiation, and vegetation type. The sensible heat modeled as

$$H = \rho_a C_p\frac{(T_l - T_a)}{R_a} \tag{5}$$

where T_l is the leaf temperature, ρ_a is the air density, C_p is the specific heat of air at constant pressure, and T_a is air temperature from the measurements made just above the canopy.

2.4. **Sensor model.** The focus of this short paper is the ground model suite described above. However, the testbed also includes atmospheric and sensor effects on the final image. The near-surface image passes through the industry-standard atmospheric radiance and transmission model, MODTRAN (*Berk et al.,* 1998), and a model to reproduce the optical blurring and sampling effects and correlated noise of the specific sensor.

2.5. **Inter-code communication and computational platforms.** The three models in the ground model suite must exchange information. The ray caster provides inbound thermal energy to the soil model and the vegetation model. They provide physical temperatures back to the ray caster. These temperatures are coupled with wavelength-dependent emissivity to estimate emitted energy from the scene. Because the codes are continuing to evolve and are each complicated in their own right, the codes were kept separate. The codes communicate using UNIX sockets at a prescribed time interval.

The problems under study present a classical need for fine spatial detail in the simulation while maintaining a large domain size to permit meaningful comparison against field data. Thus, each of the simulation codes were rewritten to function on parallel computer architectures using MPI. Although not a restriction imposed by sockets, all three codes are running on a single machine.

3. Under Development

Significant moisture movement in the shallow subsurface occurs as vapor phase transport. This need requires the simulation of air movement and precludes the use of Richards' equation. At the time of this writing, a prototype two-phase flow model has been constructed and is being transitioned to the moisture/thermal model.

Also under construction is a root zone model to represent plant uptake of water. This addition will couple the soil model and the vegetation model directly. Local variation in wind speed can affect dramatically the surface cooling for both soils and vegetation. Therefore, the current ground model suite is being extended to include a near-surface, three-dimensional air flow model.

4. Results from Initial Comparison to Field Data

The model suite has been applied to several desert sites for which field data were available. Figure 2 shows the ground surface and plant distribution in a typical synthetic scene. Data included full meteorological data, some temperature data from a column of thermistors, and thermal images from a mid-wave IR camera. Field estimates were made for bulk density, thermal conductivity, albedo, and emissivity.

The model domain was chosen to match the footprint of the boom-mounted sensor cameras. The domain was about 4 meters on a side and 1 meter deep. The spatial resolution on the ground surface was about 12 mm. Resolution was concentrated near the ground surface, decreasing quickly with depth. The resulting mesh was about 2.1 million elements for the soil and about 275,000 elements for the vegetation. A close-up showing spatial resolution on the plants and soil is shown in Figure 3.

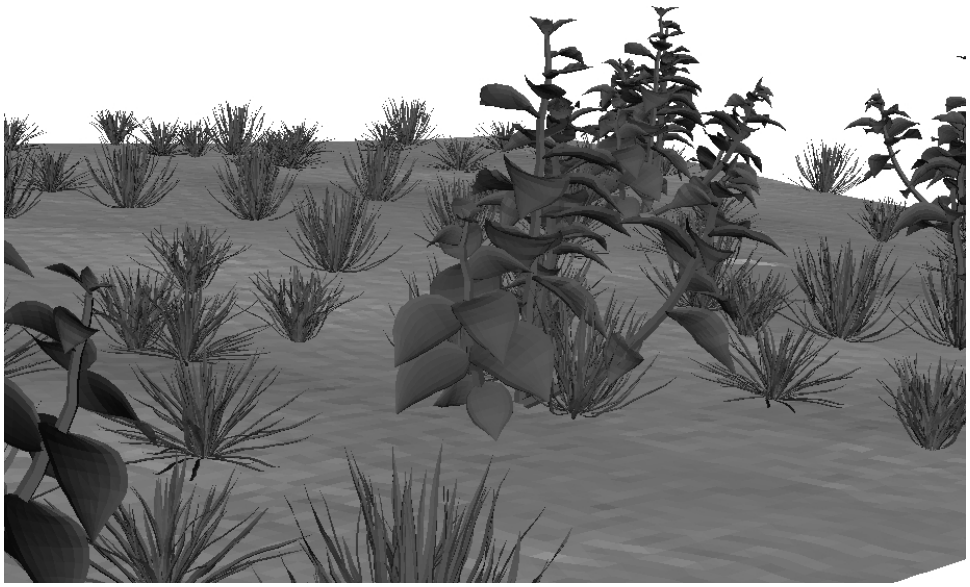

FIGURE 2. Synthetic scene showing the ground surface and both large desert plants and grasses.

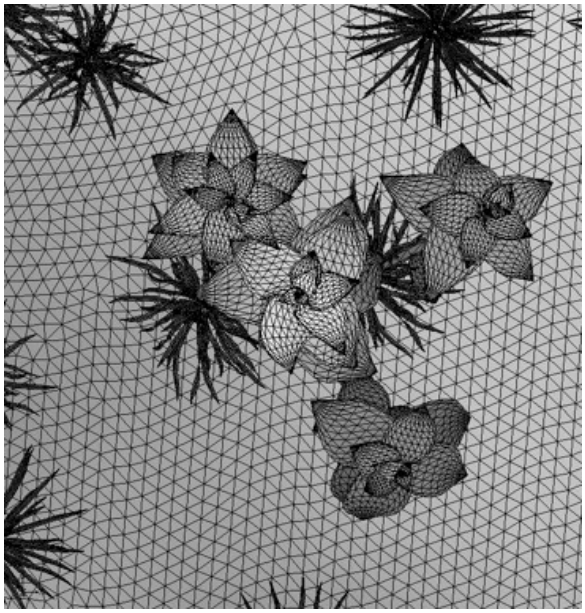

FIGURE 3. Top, close-up view of meshes used for vegetation and soil.

Unmeasured material properties were estimated using parallel PEST parameter estimation software (*Doherty,* 2000) to provide the best 'fit' between observed and computed data. The resulting 'compromise' fit to the thermistor data, while honoring apparent temperatures from the IR imagery, is shown in Figure 4.

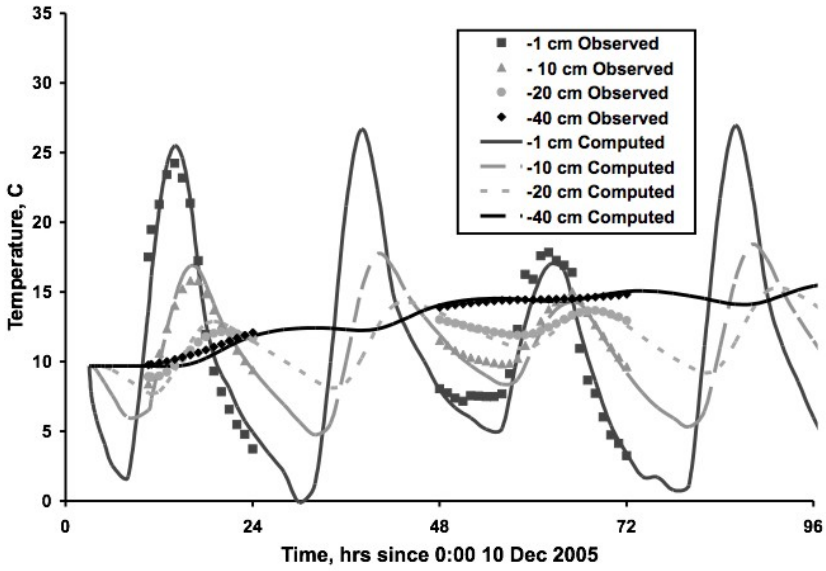

FIGURE 4. Comparison of predicted and observed physical temperatures at different depths below ground surface at the desert site.

Figure 5 shows a close-up of the three-dimensional domain with grayscale temperature contours. Cooler areas beneath the plants are created by plant shadows. The effect of these shadows propagates into the soil. Figure 6 shows a side-by-side comparison of observed and computed images. These are from a small corner of the computational domain containing no vegetation. This region was chosen to evaluate the thermal response to differences in soil properties.

FIGURE 5. Temperature contours on the vegetation and the soil. The darkest regions are cool areas caused by the plant shadows. The scene has about 4 degree C range in temperature.

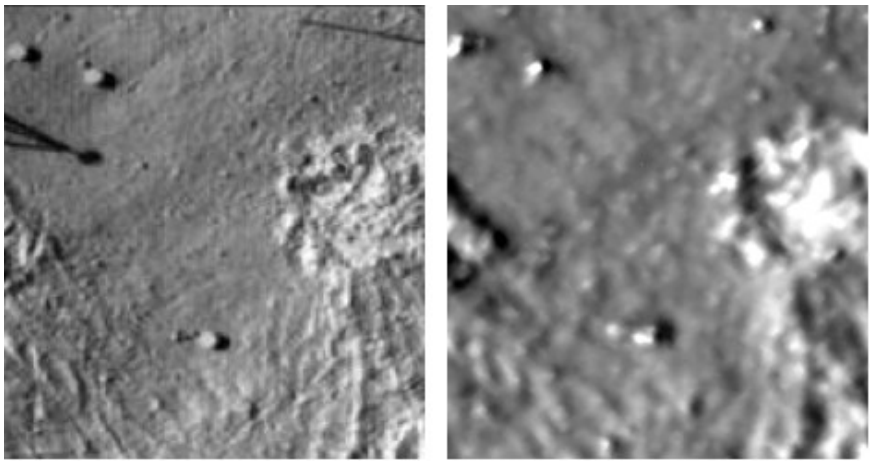

FIGURE 6. Image from a mid-wave IR camera (left) and a simulated image of physical temperatures (right).

5. Conclusions

A computational testbed was built to permit the exploration of fine-scale interaction of hydrologic and thermal processes on vegetated soil surfaces and to supplement field testing of sensor performance. The testbed produces a reasonable match to observed temperatures. A qualitative comparison between observed IR sensor images and simulated images is encouraging. A more in-depth comparison of images is underway.

Acknowledgments. Tests described and the resulting data presented herein, unless otherwise noted, were obtained from research sponsored by the Department of Defense's Institute for Maneuverability and Terrain Physics Simulation and the Countermine Phenomenology Program. Work was conducted by the Engineer Research and Development Center. Permission was granted by the Chief of Engineers to publish this information.

References

1. Berk, A., L.S. Bernstein, and D.C. Robertson (1998) "MODTRAN: A Moderate Resolution Model for LOWTRAN 7", Air Force Geophysics Laboratory Technical Report GL-TR-89-0122, Hanscom AFB, MA.
2. Doherty, J. (2000) "PEST - Model-Independent Parameter Estimation", Watermark Computing, Australia.
3. Frankenstein, S. and G. Koenig (2004), "Fast All-season Soil STrength (FASST)", Technical Report ERDC/CRREL SR-04-1, Engineer Research and Development Center, Hanover, NH, 106 pages.
4. Schmidt, J. H. (1995) *A 3-D Adaptive Finite Element Method for Transport Processes*, Master's Thesis, The University of Texas at Austin, Austin, TX.